Organic matters, but inorganic matters too: column examination of elevated mercury sorption on low organic matter aquifer material using concentrations and stable isotope ratios.

David S. McLagan[1,2,3,*], Carina Esser[1,*], Lorenz Schwab[4,5], Jan G. Wiederhold[4], Jan-Helge Richard[6], Harald Biester[1].

1 - Institute of Geoecology, Technische Universität Braunschweig, Braunschweig, 38106, Germany.

2 - Department of Geological Sciences and Geological Engineering, Queen's University, Kingston, ON, K7L3N6, Canada.

3 - School of Environmental Studies, Queen's University, Kingston, ON, K7L3J6, Canada.

4 - Department for Environmental Geosciences, Centre for Microbiology and Environmental Systems Science, University of Vienna, Vienna, 1090, Austria.

5 - Environmental Engineering Institute IIE-ENAC, Soil Biogeochemistry Laboratory, Ecole Polytechnique Fédérale de Lausanne (EPFL), Sion, Switzerland.

6 - Institute for Hygiene and Environment Hamburg, 20539 Hamburg, Germany

* - These authors contributed equally to the manuscript.

Abstract

Sorption of mercury (Hg) in soils is suggested to be predominantly associated with organic matter (OM). However, there is a growing collection of research that suggests clay minerals and Fe/Mn-oxides are also important solid-phases for the sorption of soluble Hg in soil-groundwater systems. We use a series of (60 mL syringe based) column experiments to examine sorption and subsequent desorption of $HgCl_2$ solutions (Experiment 1 [EXP1]: 46.1 ± 1.1 mg L^{-1}; and Experiment 2 [EXP2]: 144 ± 6 mg L^{-1}) in low OM (0.16 ± 0.02 %) solid-phase aquifer materials. Analyses of total Hg concentrations, Hg speciation (i.e., pyrolytic thermal desorption (PTD)), and Hg stable isotopes are performed on both solid- and liquid-phase samples across sorption and desorption phases.

Sorption breakthrough curve best fitted a Freundlich model. Despite the very low OM content, the Hg equilibrium sorptive capacity in these columns is very high: 1510 ± 100 and 2320 ± 60 mg kg^{-1} for the EXP1 and EXP2, respectively, and is similar to those determined for high OM soils. Data from the experiments on mass dependent fractionation of Hg stable isotope fractionation data (described by $\delta^{202}Hg$) support preferential sorption of lighter isotopes to the solid-phase materials with results indicating isotopically heavier liquid-phase and isotopically lighter solid-phase. Desorption fits exponential decay models and 46 ± 6% and 58 ± 10% of the sorbed Hg is removed from the solid-phase materials at the termination of desorption in EXP1 and EXP2, respectively. The divergence of $\delta^{202}Hg$ values between liquid- and solid-phase also continues into desorption. This desorption profile is linked to the initial release of easily exchangeable Hg(II) species physically sorbed to Fe/Mn-oxides and clay mineral surfaces (liquid-phase enriched in heavy isotopes) and then slower release of Hg(II) species that have undergone secondary reaction to more stable/less soluble Hg(II) species and/or diffusion/transport into the mineral matrices (processing favouring lighter isotopes; solid-phase enriched in lighter isotopes). ~~Hg stable isotope support preferential sorption of lighter isotopes to the solid-phase materials with results indicating isotopically heavyier liquid-phase and isotopically lighter solid-phase. The divergence of $\delta^{202}Hg$ (describing mass dependent fractionation (MDF)) between liquid- and solid-phase continues into desorption and we attribute this to lighter isotopes being favoured in secondary processes occurring after initial sorption to the solid-phase materials (i.e., matrix diffusion, change in Hg(II) speciation, elemental Hg (Hg(0)) production) that lead to less exchangeable forms of Hg. Consequently, heavy isotopes are preferentially released during desorption. These observations agree with data from $HgCl_2$ contaminated sites.~~ The secondary production of Hg(0) within the columns is confirmed by PTD analyses that indicate distinct Hg(0) release peaks in solid-phase samples at <175 °C, which again agree with field observations. Retardation (R_D) and distribution (K_D) coefficients are 77.9 ± 5.5 and 26.1 ± 3.0 mL g^{-1} in EXP1, respectively, and 38.4 ± 2.7 and 12.4 ± 0.6 mL g^{-1} in EXP2, respectively. These values are similar to values derived from column experiments on high OM soil and provide the basis for future Hg fate and transport modelling in soil-groundwater systems.

Keywords: Mercury stable isotopes, column experiments, sorption/desorption, groundwater, polluted sites, distribution coefficient.

1 Introduction

Mercury (Hg), a transition metal of group 12 and period 6 of the periodic table, has a unique electrochemical structure. The pair of electrons in the outermost (6s) shell have a relativistically contracted radius, which greatly reduces the element's ability to form metal-metal bonds (Norrby, 1991). Hence, Hg is the only liquid-phase metal at standard temperature and pressure. Even with

this radial contraction, Hg is an atomically large element, and species in its divalent oxidation state qualify as "soft-acids", which under hard and soft Lewis acid and base theory results in Hg having greater affinity for "soft-bases" (Ho, 1975). One particularly pertinent "soft-base" for Hg is sulphur. Cinnabar (α-HgS) and meta-cinnabar (β-HgS) are the dominant forms of Hg in the lithosphere (Gettens et al., 1972; Clarkson, 1997), but are relatively stable ores that~~,~~ have very low solubility, and ~~low~~ bioavailability (Llanos et al., 2011; Lu et al., 2011). Mining of these cinnabar ores for industrial use of Hg has heavily perturbed the natural biogeochemical cycle of Hg. Other primary sources of Hg emissions/releases to the environment include geogenic (natural), fossil-fuel combustion, industrial and medical uses of Hg, and legacy emissions from Hg polluted sites (Pirrone et al., 2010; Kocman et al., 2013; Streets et al., 2019).

While redox conditions and organic matter (OM) availability and composition are key determinants in the mobility of Hg in aquatic/saturated subsurface environments, pH (Andersson, 1979; Gu et al., 2011; Manceau and Nagy, 2019), chloride concentration (Cl^-; Schuster, 1991), and speciation of Hg inputs (particularly for polluted systems; McLagan et al., 2022) also play important roles. Solubilities of Hg species vary widely from practically insoluble cinnabar species (≈ $2*10^{-24}$ g L^{-1}) to low solubility elemental Hg (Hg(0): ≈ $5*10^{-5}$ g L^{-1}) to highly soluble Hg(II)-chloride ($HgCl_2$) (66 g L^{-1}) (Sanemasa, 1975; Schroeder and Munthe, 1998; Skyllberg et al., 2012). In systems that are OM limited, clay minerals and oxides, hydroxides, and oxyhydroxides of Fe, Mn and Al become increasingly important sorbents for Hg species (Lockwood and Chen, 1973; Schuster 1991; Kim et al., 2004). Additionally, there is a strong tendency of Hg(II) to complex with hydroxides and halides under oxic conditions (Schuster, 1991, Ullrich et al., 2001). Uptake of Hg to inorganic sorbents has been reported to occur via rapid initial surface sorption followed by slower phase of Hg undergoing secondary transformation to more stable/less soluble species or diffusing into the mineral matrices (Avotins, 1975; Miretzky et al., 2005; McLagan et al., 2022).

More recently, laboratory and field studies have expanded biogeochemical assays of Hg in subsurface environments using stable isotopes (Jiskra et al., 2012; Zheng et al., 2018; McLagan et al., 2022). Hg is an isotopic system that has seven stable isotopes and to which environmental processes can impart mass-dependent (MDF) as well as both odd and even mass-independent (MIF) fractionation (Bergquist and Blum, 2007; 2009; Wiederhold, 2015). In particular, this capacity for Hg stable isotope analyses to elicit valuable information on tracing/identifying specific environmental processes make them a vital tool in the examination of Hg biogeochemical cycling (Bergquist and Blum, 2007; 2009; Wiederhold, 2015).

Traditionally, column and batch experiments have been utilised to assess the sorption (including sorption or distribution coefficient: K_D and the related retardation coefficient: R_D) and mobility of contaminants for solid-phase soil and aquifer materials. Both methods have strengths and weaknesses. Batch experiments represent the simplest means to test analyte sorption, but these experiments are static, and equilibrium oriented; questions about the applicability of the results to natural systems with flowing water and potentially changing levels of saturation logically persist (Schlüter et al., 1995 Schlüter, 1997; Van Glubt et al., 2022). Flow-through columns provide a much more dynamic and manipulatable experimental environment that is also not exclusively limited to equilibrium-based sorption simulations. Nonetheless, they are more laborious, difficult to replicate from column to column, column boundaries (walls) can present preferential flow problems, and despite the ability to manipulate the physicochemical properties of the columns this inevitably underrepresents the inherent variability of actual soil/aquifer conditions (Sentenac et al., 2001;

USEPA, 2004). Soil contaminant transport modelling is a rapidly developing field of research and provides an alternative/complementary method to these traditional experimental methods. While Hg soil transport modelling is also advancing, progress is somewhat limited by the lack of measurement data particularly relating to K_D values, Hg speciation and methods of assessing specific processes for different soil/solid-phase materials (Leterme et al., 2014; Richard et al., 2016a).

Thus, it is important from both experimental and modelling standpoints that we determine effective means of deriving information on sorption/mobility of Hg in soils. Lacking the capacity to measure aquifer systems *in-situ*, we deem column experiments using solid-phase materials sourced from sites of interest as the best available method to do so. Within this study, we aim to determine the sorptive (and desorptive) capacity of low OM aquifer materials for Hg(II) using column experiments and total Hg (THg) concentration, speciation, and stable isotope analyses of both solid and liquid-phase materials. These experiments will be the first conducted on such low OM soil/aquifer material and provide critical data into Hg transport and sorption within low OM soil and aquifer systems to improve our geochemical understanding of subsurface Hg behaviour and for soil chemistry and transport modelling. In addition, these column experiments on uncontaminated aquifer material sourced from an area adjacent to a former industrial site at which $HgCl_2$ was applied as wood preservative will simulate the contamination process. Data will aid our interpretation of the Hg biogeochemistry in coupled soil-groundwater systems, as well as future Hg groundwater transport modelling, and potentially provide guidance on contaminated site remediation.

2 Methods

2.1 Materials and experimental setup

The solid-phase material used in these experiments is highly permeable sand-gravel sediments sourced from the saturated zone of an unconsolidated aquifer (approximate depth: 10 m) extracted by a soil drill core in 2019. This site was impacted by losses of approximately 10-20 tonnes of Hg in the form of high concentration $HgCl_2$ solution (≈0.66% $HgCl_2$) that was applied to timber as a preservative (Schöndorf et al., 1999; Bollen et al., 2008; McLagan et al., 2022). The solid-phase materials were extracted from outside of the plume of contaminated groundwater (Site B in McLagan et al., 2022); and hence, the starting THg concentration within was very low (Table 1). The geology and structure of the soil/aquifer profile has been described in detail in previous works (Schöndorf et al., 1999; Bollen et al., 2008; McLagan et al., 2022). The material was stored in a dark and cool place before drying at 30 °C for 48 hours. It was then sieved to a size of <2 mm using a mesh soil sieve, which resulted in a distribution of 74.1 ± 4.6% coarse load (>2 mm; not used) and 25.8 ± 4.6% fine load (<2 mm). A subsequent particle size analysis of the fine load was carried out using sieving and sedimentation method (DIN ISO 11277, 2002), and results (see Table 1) categorise the solid-phase aquifer materials as a sandy-loam on the soil texture triangle. A summary of the properties of the investigated material is shown in Table 1.

Table 1: Properties of the solid-phase aquifer material used.

Parameter	Fe ($g\ kg^{-1}$)	Mn ($mg\ kg^{-1}$)	Hg ($\mu g\ kg^{-1}$)	TC (%)	TOC (%)	TIC (%)	Clay (%)	Silt (%)	Sand (%)
Value	19.2 ± 1.5	690 ± 160	20.4 ± 1.0	0.50 ± 0.03	0.16 ± 0.02	0.34 ± 0.03	13.5	23.2	63.3
Samples (*n*)	16	16	6	3	3	3	1	1	1

A set of preliminary experiments prior to experiment 1 (EXP1) and experiment 2 (EXP2) were run to optimise packing methods, flow rates, stock solution concentration, and time the experiments would take, and these are detailed in Section S1. Based on these preliminary data the experimental setup was based on a modified version of DIN method 19528-01 (DIN 2009). 8 x 60 mL disposable polypropylene syringes (height: 15.49 cm; inner diameter: 2.97 cm) were used as columns in each experiment (Figure 1). The insides of the columns were roughened with sandpaper (and thoroughly cleaned with surfactant and rinsed with deionised~~DI~~ water to remove any debris) in order to minimise preferential flow along the walls of the column. Each column was then filled with a layer of quartz wool and a layer of quartz beads whose combined volume reached the 10 ml mark on the syringe. The sieved and dried material was then transferred by ≈14 g aliquots into the syringes (preliminary testing revealed dry packing achieved optimal column density and was best at preventing separation). Each aliquot was compacted to the desired volume and the surface of each aliquot was broken up before the addition of the subsequent aliquot to prevent layering between each addition. The mean mass and bulk density (ρ_b) of the solid-phase aquifer materials added to the columns was 70.09 ± 0.04 g and 1.42 ± 0.01 g cm^{-3}, respectively, in EXP1, and 70.05 ± 0.03 g and 1.43 ± 0.01 g cm^{-3}, respectively, in EXP2. This resulted in the height of the solid-phase materials within the column being ≈11 cm. Additional layers of quartz beads then quartz wool (syringe volume again ≈10 mL) were added on top of the solid-phase materials to reduce column separation and particle transport. Individual columns are named~~s~~ C1.1 to C1.8 for EXP1 and column C2.1 to C2.8 in EXP2. According to Lewis and Sjöstrom (2010), the average bulk densities range from 1.2 – 2.0 g cm^3 for sands and 1.6 – 2.0 g cm^3 for gravel. Thus, we deem the achieved bulk density of the columns to be appropriate for these materials, particularly as densities of the removed coarse materials are higher (solid densities are estimated at 2.65 g cm^3; Lewis and Sjöstrom (2010)).

All column experiments were conducted under saturated conditions. Figure 1A shows the configuration of the setup with the peristaltic pump upstream of the columns and flow through the columns was bottom to top to minimise entrapment of air and preferential flow paths. The stock solution, peristaltic pump, columns, and eluate sampling points were connected with 3.125 mm (inner-diameter) polypropylene tubing (length: 105 ± 10 cm; *n* = 16). To simulate the aquifer (flow velocity of ≈3 – 10 m day; Schöndorf et al., 1999; Bollen et al., 2008) and prevent separation of the solid-phase materials within the column, the lowest possible volume flow of 0.62 ± 0.02 ml min^{-1} (*n* = 16) was set across all columns (flow velocities measured before and after experiments; Section S2). The stock solution was made using mixing $HgCl_2$ salt with tap water and stored in a 20 L polyethylene container. Tap water was selected due to its inherent concentration of ions, low potential for biological activity, and ease-of-use (challenges in extraction, storage, and transport of large groundwater volumes from study site ≈600 km away). Critically, the tap water and eluate DOC concentrations (2.3 – 3.3 mg L^{-1}) were of a similar range (even slightly less) than the values measured by Richard et al (2016a) at the site these solid-phase materials were removed (3.8 – 6.3 mg L^{-1}). This should eliminate the possibility that tap water would introduce a significant amount of artificial sorption sites associated with DOC being added to the system.

Stock solutions were 46.1 ± 0.1 mg L^{-1} in EXP1 (*n* = 6) and 144 ± 6 mg L^{-1} in EXP2 (*n* = 12) and were selected for (i) experimental constraints/time considerations (see Figure S1.6) and (ii) these values remain between $HgCl_2$ concentration applied during industrial activities (6600 mg L^{-1}; spillages of this solution to the top of the soil profile) and ~~as estimates of the original concentrations of $HgCl_2$ contaminated solution entering the soil-groundwater system considering~~ recently measured

groundwater concentrations up to 164 ± 75.4 µg L^{-1} ~~are still~~ observed 55 years after ~~closure~~ cessation of the industrial activities at the site ~~the solid-phase materials were extracted~~ (McLagan et al., 2022). The physicochemical properties of both the stock solutions and eluate were monitored across the experiments and data are listed in Section S2. Desorption was performed by replacing the stock solution with tap water flowing at the same velocity. In total (sorption, equilibrium, and desorption), EXP1 and EXP2 ran continuously for 14 days, 3 hours, and 9 minutes, and 10 days, 13 hours and 4 minutes, respectively.

Columns were pre-conditioned with tap water for 1 week at the experimental flow velocity to allow equilibration between the solid-phase materials and the dissolved substances in the tap water, the major component of the stock solution used within the experiment. After 24 hours of pre-conditioning, NaCl salt solution tracer experiments were conducted to monitor the rate of water transfer through the columns (assuming NaCl is a conserved tracer that does not interact with the solid-phase materials). The NaCl solution was passed into the system for 10 minutes and then replaced with tap water. The change in conductivity was measured over time using a hand-held electronic conductivity meter to produce NaCl (tracer) breakthrough curves. Results show good column flow consistencies similar to the volumetric flow measurements and both data sets are described in detail in Sections S1 and S2. The system was rigorously tested and checked for leaks during both the pre-conditioning and testing phases.

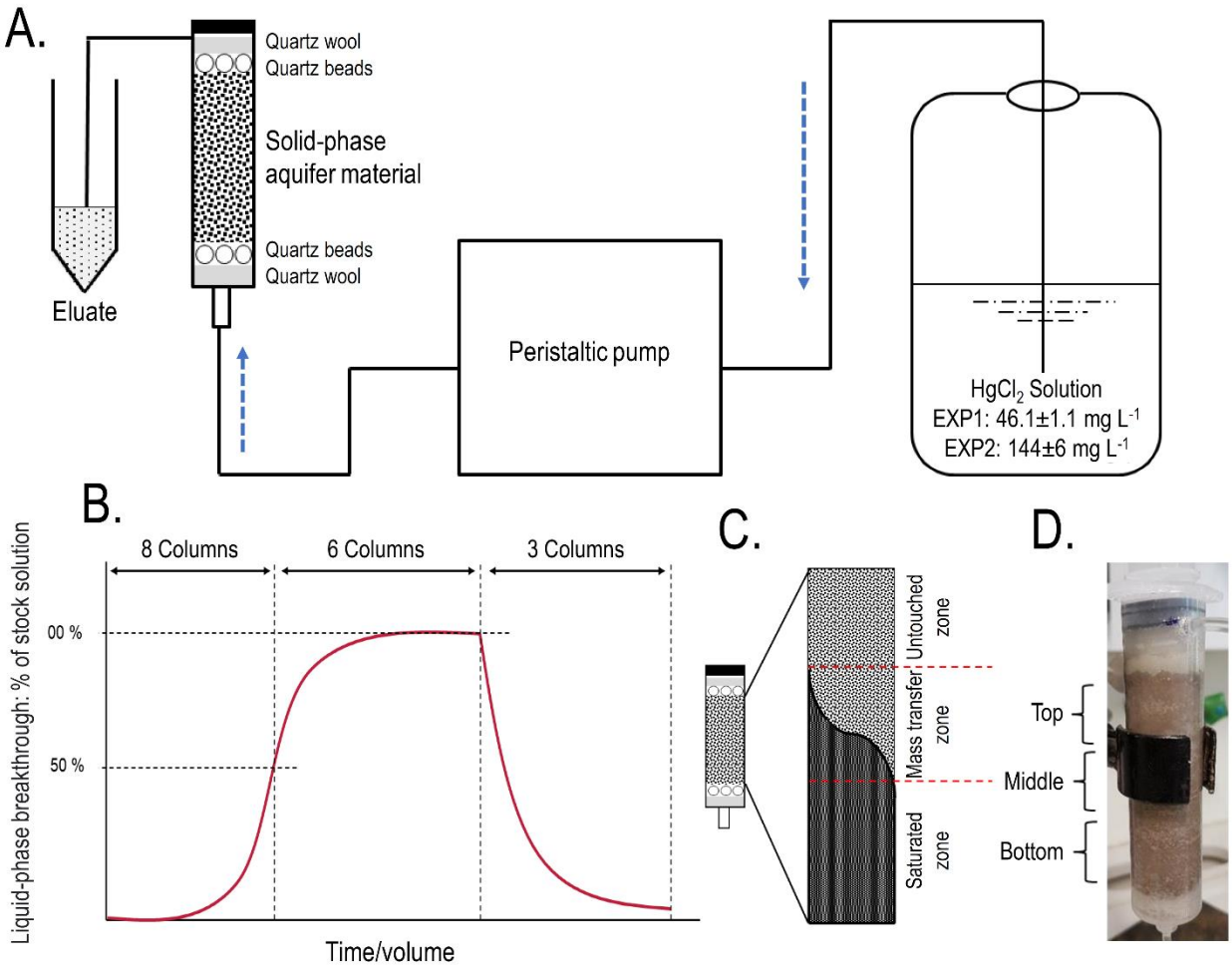

Figure 1: A. Schematic representation of the experimental setup. B. Theoretical model of the experiments indicating sorption and desorption phases and column termination points for solid phase analyses (2 columns terminated at 50 % breakthrough, 3 columns terminated at ≈equilibrium,

and the final 3 columns terminated after desorption; end of experiment). C. Representation of the zones of mass transfer of Hg during the sorption phase ("saturated zone" refers to solid-phase in that zone reaching its equilibrium uptake capacity for Hg at the experimental solution concentration). The dark area describes the rising front of mercury. D. Allocation of column sections (≈15 mL in each section) for solid-phase analyses ("Bottom" is the solution entry point).

10 mL of eluate was allowed to flow off into a waste vessel before 5 mL of sample was collected~~ion periods~~ for analysis (this applied to all analyses). The liquid-phase was sampled for ~~total Hg (~~THg~~)~~ concentrations consistently throughout the experiments: 38x in EXP1 (10x up to ≈50% breakthrough – columns C1.1-C1.8; 11x between ≈50% breakthrough and ≈equilibrium – columns C1.1-C1.6; and 17x during desorption – columns C1.1-C1.3) and 35x in EXP2 (8x up to ≈50% breakthrough – columns C2.1-C2.8; 16x between ≈50% and ≈100% breakthrough – columns C2.1-C2.3 and C2.6-C2.8; and 11x during desorption – columns C2.1-C2.3). Liquid-phase speciation samples were collected 8x at ≈25%, 50%, 75% breakthrough, and ≈equilibrium, at the end of the equilibrium (immediately before stock solution was changed to tap water), and ≈0% (immediately after stock solution was changed to tap water), 50% and at the end of desorption for both experiments. Liquid-phase stable isotope samples were collected only from columns C2.1-C2.3 in EXP2 9x in total. Collections were similar to liquid-phase speciation sampling points with an additional collection during the sorption stage of the experiment. After termination, solid-phase materials were analysed for THg concentrations, Hg species, and Hg stable isotopes. In summary, C1.7 and C1.8 and C2.4 and C2.5 were sacrificed at ≈50% breakthrough; C1.4-C1.6 and C2.6-C2.8 after equilibrium (≈100% breakthrough); while C1.1-C1.3 and C2.1-C2.3 went through to the end of desorption.

2.2 Analyses

2.2.1 Liquid-phase THg and speciation analyses

Eluate samples for THg and Hg stable isotope analyses were immediately stabilized by adding 1% by volume of 0.2 M bromine monochloride (BrCl) prepared according to Bloom et al. (2003). In order to break up all of the organically bound mercury in the liquid, a reaction time of the BrCl of 24-hours is recommended (US EPA method 1631, 2002). However, with little OM (Table 1), we assessed sample THg analysis only 1-hour after BrCl addition and there was no impact on sample recovery (Table S1.2). Immediately prior to analysis, hydroxylamine hydrochloride ($NH_2OH{\cdot}HCl$) was added to neutralize the BrCl followed by addition of tin(II) chloride ($SnCl_2$) solution as the Hg reducing agent.

Liquid-phase speciation analyses followed the same methods described elsewhere (Bollen et al, 2008; Richard et al., 2016b; McLagan et al., 2022). We describe this method ~~is described~~ as a complementary, semi-quantitative ~~qualitative~~ analytical tool and produces four distinct "fractions" of the total pool of liquid-phase Hg: (i) elemental Hg (Hg(0)) (purged from untreated eluate sample), (ii) dissolved inorganic Hg(II) termed Hg(II)A; (purged after reduction with $SnCl_2$ treatment; e.g. $HgCl_2$); (iii) DOM-bound Hg(II) termed Hg(II)B (purged after BrCl and $SnCl_2$ treatment), and (iv) particulate Hg termed Hg(II)P (difference between THg concentrations in filtered and total unfiltered eluate samples). Both concentration and speciation results were measured using a cold-vapor atomic absorbance spectrometer (CV-AAS) (Hg-254 NE, Seefelder Messtechnik GmbH, Germany) according to DIN method 1483 (2007) and USEPA method 1631 (2002). Confidence in liquid phase Hg(0) concentrations is higher than for other species, as these result from purging untreated/unstabilised samples of Hg(0) with nitrogen gas directly into the CV-AAS; all Hg(0) samples were analysed within 30 mins of sample collection.

2.2.2 Solid-phase THg and speciation analyses

After individual columns were sacrificed for solid-phase analyses, the ends of the columns were sealed to prevent the columns from draining and stored in the same upright position as the experimental setup (Figure 1) to prevent further disturbance. Columns were cut into sections (Figure 1D), homogenised and subset within 1 week of the end of the experiments and stored at 4 °C in brown (opaque) falcon tubes until digestions or analyses. All analyses were performed on wet samples to minimise any potential losses of Hg(0)~~All analyses were performed on wet samples to ensure there were no losses of Hg(0)~~. The moisture content of solid-phase samples was determined on separate aliquots for each column by difference after drying at 35 °C and was 23 ± 2% (n = 48) (Section S8).

THg and Hg stable isotope analyses were cold digested in modified aqua regia following the methods described in McLagan et al. (2022) (8 mL HCl, 3 mL HNO_3, and 1mL BrCl~~1 mL nitric acid replace with 1 mL BrCl~~). Analyses of THg concentrations from the digestion extracts were determined using CV-AAS following DIN method 1483 and USEPA method 1631. Results are reported on a dry weight basis and moisture content was determined by difference after baking at 105 °C using aliquots of the solid-phase sample (Section S8). Due to the low concentrations in the original solid-phase aquifer materials, THg concentrations were measured with a DMA80 (Milestone SCI) via thermal decomposition, amalgamation, and AAS (Table 1).

Speciation analyses were performed by pyrolytic thermal desorption (PTD), which continually measures Hg at 254 nm within an AAS detector that is connected to a sample combustion furnace that heats samples from room temperature to 650°C a 1°C per minute in a stream of N_2 gas. This method is described in detail by Biester and Scholz (1996). The sample release curves were compared to the release curves for a series of Hg reference materials (Hg(0), $HgCl_2$, Hg_2Cl_2 (calomel), cinnabar: α-HgS, metacinnabar: β-HgS, and Hg^{2+}-sulphate: $HgSO_4$) in silicon dioxide (SiO_2) matrix (see Section S9 for reference material curves) to qualitatively assess the species or "fractions" of Hg present in the samples.

2.2.3 Liquid- and solid-phase Hg stable isotope analyses

Samples for stable Hg isotope analyses included stabilized liquid-phase eluate samples and solid-phase aqua-regia extracts diluted with deionised water (18.2 MΩ cm). Liquid-phase samples were collected in 15 mL polypropylene tubes and stabilized with BrCl to reach 1% of the sampled volume. Analyses were made using a Nu Plasma II (Nu Instruments) multicollector inductively coupled plasma mass spectrometer (MC-ICP-MS) with a cold-vapor generator (HGX-200; Teledyne Cetac) that allows direct addition of Hg(0) into MC-ICP-MS plasma by reducing all Hg in samples with $SnCl_2$. The isotope ratios were determined relative to NIST-3133 (National Institute of Standards and Technology; NIST) using the standard bracketing approach and corrected for mass-bias using thallium (Tl) doping from NIST-997 (NIST) introduced using an Aridus-2 desolvating nebulizer (Teledyne CETAC). MDF was assessed by variation in $\delta^{202}Hg$, while $\Delta^{199}Hg$, $\Delta^{200}Hg$, $\Delta^{201}Hg$, and $\Delta^{204}Hg$ were used to assess MIF of odd and even isotopes) (see Grigg et al., 2018; McLagan et al., 2022 for method details).

2.2.4 Complementary analyses

Metal cations in the solid- and liquid-phases were measured with inductively coupled plasma optical emission spectrometry (ICP-OES; Varian 715-ES; Agilent Technologies Inc.). Solid-phase total carbon

(TC), total organic carbon (TOC), and total inorganic carbon (TIC; dissolved by hydrochloric acid) were measured by infra-red detection of CO2 released (DIMA 1000NT; Dimatec, Germany). Dissolved organic carbon of stock solution and eluate was measured with a carbon/nitrogen analyser (Multi N / C 2100; Analytic Jena) (see Section S2). Liquid-phase dissolved oxygen content, redox potential, electrical conductivity, and pH were measured by handheld probes.

2.2.5 Retardation (R_D) and sorption/partitioning/distribution (K_D) coefficient calculations

The retardation coefficient (R_D) is essentially the ratio of the velocity of the water front (v_w) and velocity of the Hg front delayed by sorption processes (v_{Hg}) moving through the columns (Equation 1). Since the path of the the soluble pollutant (Hg) and water are the same, transport time can be determined based on the time it takes the fronts to pass through the columns (t_{Hg} and t_w, respectively). NaCl breakthrough curve was used as a proxy for water based on the assumption it is a conservative tracer. t_{Hg} and t_w are given when the respective ratios of the NaCl and THg concentrations in the eluate is equal to half the input concentration (stock solution; C_{eluate} / $C_{initial}$ = 0.5) (Patterson et al., 1993; Reichert, 1991; Schnaar and Brusseau, 2013).

$$R_D = {}^{v_w}/_{v_{Hg}} = {}^{t_w}/_{t_{Hg}} \quad \text{Equation 1}$$

R_D is related to the sorption or partitioning or distribution coefficient (K_D; mL g^{-1}) according to Equation 2 and Equation 3 (USEPA, 2004):

$$R_D = 1 + ({}^{\rho_b}/_{n_e})K_D \quad \text{Equation 2}$$

$$K_D = (R_D - 1)({}^{n_e}/_{\rho_b}) \quad \text{Equation 3}$$

Where, n_e is the effective porosity (EXP1: 0.470 ± 0.008, n = 3; EXP2: 0.459 ± 0.004, n = 3; assumed to be equal to total porosity), which is the ratio of the column pore volume (EXP1: 23.3 ± 0.5 mL, n = 3; EXP1: 22.5 ± 0.1 mL, n = 3) to the total volume of the solid-phase materials of the columns (EXP1: 49.7 ± 0.3 mL, n = 3; EXP2: 49.0 ± 0.5 mL, n = 3). R_D could only be calculated for columns that went to equilibrium and desorption (not 50% breakthrough), n_e was calculated for columns that went through desorption (C1.1-C1.3 and C2.1-C2.3); and hence, K_D was only calculated for these columns. Note, the pore volumes reported above are the data used when reporting the number of pore volumes.

2.3 Quality Assurance and quality control (QAQC)

For liquid-phase analyses, a 140.8 ng L^{-1} Hg(II) stock solution (Sigma Aldrich) was measured throughout the analyses and recovery was 99 ± 5% (n = 250). For solid-phase analyses, Chinese Soil (NCS DC73030; Chinese National Analysis Centre for Iron and Steel) was measured and recovery was 101 ± 6% (n = 16). The accuracy and precision of Hg stable isotope measurements was assessed using the "in-house" *ETH Fluka* standard. Mean values across the measurement sessions were: δ^{202}Hg = -1.42 ± 0.08 ‰; Δ^{199}Hg = 0.08 ± 0.02 ‰; Δ^{200}Hg = 0.02 ± 0.02 ‰; Δ^{201}Hg = 0.03 ± 0.03 ‰; Δ^{204}Hg = -0.01 ± 0.06 ‰ (n = 26; all uncertainty values are reported as 2SD). All uncertainties are 1SD, unless otherwise reported (i.e., 2SD used to report Hg stable isotope analysis uncertainty). These values are within the range of other studies (i.e., Obrist et al., 2017; Goix et al., 2019; McLagan et al., 2022). Theoretical solid-phase THg concentration (compared to measured THg concentrations) are determined via mass balance of liquid-phase THg concentrations of stock

solution and eluate and the volume of stock solution applied to the columns. All statistical tests and sorption fitting comparisons were performed in OriginPro 2018 (Origin Lab Corporation).

3 Results and discussion

3.1 Sorption and desorption behaviour of mercury in column experiments

3.1.1 Sorption

As expected, the uptake of the $HgCl_2$ solution to the solid phase aquifer materials followed an *S-shaped* breakthrough curve best described by ~~the~~ a Freundlich function~~model~~ (Figure 2; note these are empirically fitted functions). Initially, >99.9% of the Hg in solution was sorbed to the solid phase materials and 1.0-1.3 L (43 – 55 pore volumes) and 0.3-0.45 L (13 – 16 pore volumes), in EXP1 and EXP2, respectively, was required to reach eluate THg concentrations equivalent to 1% of stock solution (Section S5). This was followed by a phase of rapid increase in the eluate concentrations (decreasing fraction of the Hg in solution sorbing to the solid-phase). Finally, the increase in eluate THg concentration slowed as it approached the upper asymptotic bound of the original stock solution concentration in each experiment and equilibrium of Hg fluxes between the solid- and liquid-phases was approached/reached. EXP1 likely did not completely reach a stable equilibrium point (eluate concentration was at ≈91% of stock solution concentration when the stock solution was changed to water), and more time/volume of solution was required. This would have required creation of more stock solution; instead, green chemistry prevailed, and the choice was made to move onto the desorption phase with consideration of the higher concentration (faster) follow-up EXP2.

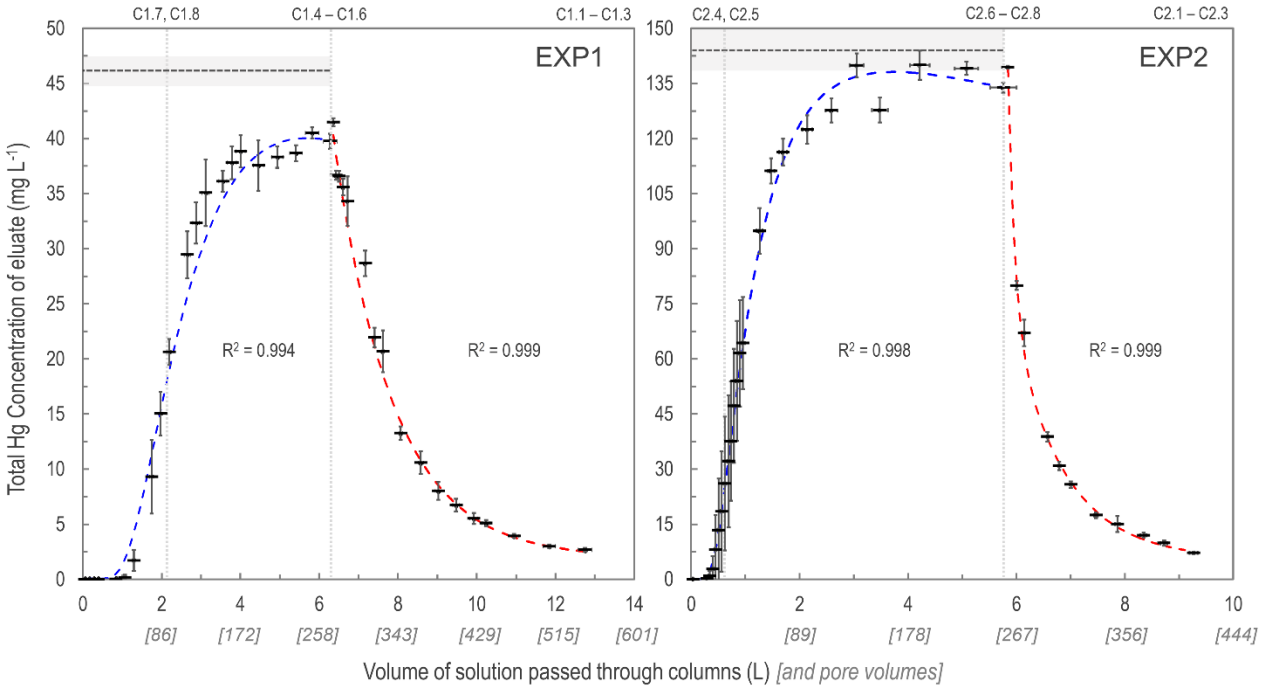

Figure 2: Total Hg concentration eluate breakthrough curves for low (EXP1; left panel) and high (EXP2; right panel) concentration stock solution experiments. Horizontal dashed lines (mean) and shaded area (1SD) indicate the original stock solution concentrations in each experiment and vertical dotted lines indicate column removal points (column IDs above panels indicate which columns were removed). Uncertainty in the x-axis relates to the differing volumes passed through individual columns at each sampling period. Sorption curves were fitted with Freundlich functions (blue dashed lines), and desorption curves were fitted with exponential decay functions (red dashed lines). These

functions were empirically (not mechanistically) fitted to the data as these plots are not sorption isotherms (see. These relationships presented the best fits compared to the fit of sorption functions and full details of these functions are listed in Section S6 for details of fitting functions).

This *S-shaped* sorption behaviour was similar to the one other detailed study on Hg sorption in natural soils with sufficient liquid-phase sampling frequency to create column breakthrough curves on OM-rich (9.4 – 24.7% OM) Amazonian soils and similar stock solution concentrations (60 – 120 mg L^{-1}; Miretzky et al., 2005). ~~Qualitative~~ Semi-quantitative liquid-phase Hg speciation analyses confirm that the majority of Hg was dissolved inorganic Hg(II) (EXP1: 83 ± 6%; EXP2: 77 ± 8%), a fraction of which will be soluble $HgCl_2$ (species used to generate stock solution), but also fractions of hydrolysed species (i.e., HgClOH, $Hg(OH)_2$, $[HgCl_3]^-$) formed in solution at pH in the observed range (7.7 – 8.1) of these experiments (Delnomdedieu et al., 1992; Gunneriusson and Sjöberg, 1992; Kim et al., 2004; see also Section S10 for theoretical Hg speciation results using Visual MINTEQ v3.1). These liquid-phase Hg speciation results are similar to those reported for groundwater samples previously collected at the contaminated site where these materials were extracted from (Bollen et al., 2008; Richard et al., 2016a; McLagan et al., 2022).

Despite the very low OM content (Table 1) within these solid-phase aquifer materials, the equilibrium uptake capacity was very high in both experiments. These concentrations were determined both (i) analytically by solid-phase THg analyses, and (ii) theoretically, based on the inverse of the breakthrough curve integral: the area above the curve and below the stock solution concentration. This has been referred to as "holdup" (*H*; mg of Hg), (Van Genuchten and Parker, 1984) and is described in Equation 4:

$$H = [C_0 V_f - \int C_e \, dV] \qquad \text{Equation 4}$$

Where, C_e is the eluate THg concentration (mg L^{-1}), C_0 is the stock solution THg concentration (mg L^{-1}), and V_f is the accumulated solution volume that has passed through the columns at the point they were removed (L). Theoretical concentrations reached 1880 ± 20 mg kg^{-1} in EXP1 and 2810 ± 40 mg kg^{-1} in EXP2 (Table 2; Section S3). These data are directly comparable, and indeed within the same range as the theoretical solid-phase concentrations calculated by Miretzky et al. (2005) for the OM-rich Amazonian soils (THg concentrations: 950 – 3960 mg kg^{-1}). The elevated Hg sorption observed by Miretzky et al. (2005) is to be expected due to the affinity of Hg for OM (e.g., Yin et al., 1996; Jiskra et al., 2015; Manceau and Nagy, 2019). Nonetheless, Miretzky et al. (2005) found their calculated solid-phase THg concentrations at equilibrium (sorptive capacity of the soils) were greater when OM% + clay% was considered rather than OM% alone was considered (Miretzky et al., 2005), which highlights the potential role clay (and oxide) minerals can play in Hg sorption to solid-phase soil or aquifer materials.

Hg sorption to OM has been observed to increase at lower pH (Andersson, 1979; Yin et al., 1996). However, the opposite has been reported for sorption of Hg to clay minerals: in neutral and slightly basic soils, the sorption capacity is controlled by the mineral components (Andersson, 1979; Schuster, 1991; Gabriel and Williamson, 2004). Indeed, the pH range of the eluate and stock solution (pH range: 7.7 – 8.1) present ideal conditions for Hg sorption to clay minerals and Fe and Mn (oxy)hydroxide minerals. Hg sorption to these inorganic minerals becomes more likely in our experiments considering the very low OM content of the solid-phase materials (Table 1). Haitzer et al. (2002) estimated that at ratios of THg-to-OM above 1 µg of Hg per mg of OM the strong thiol-group bonding sites for Hg within OM are saturated. Based on the TOC data of these solid-phase

materials (assuming 0.16% TOC = 0.32 % OM), there would be 224 mg of OM within a column. To surpass the ratio of 1 µg of Hg per mg of OM, only 4.9 and 1.6 mL of stock solution or 0.21 and 0.07 pore volumes in EXP1 and EXP2, respectively, would need to be added to the columns to saturate the strong thiol-group binding sites with Hg. Considering that Hg breakthrough occurred only after about 50 and 15 pore volumes in EXP1 and EXP2, respectively, it can be assumed that not only the strong Hg-binding thiol-groups but also the other less strong Hg-binding functional groups (e.g., carboxyl groups) of the small OM pool in the columns were fully saturated early in the experiments. Hence, solid-phase sorption of Hg within these experiments was dominated by interactions with inorganic minerals. The role of such inorganic minerals was also highlighted in one of the few studies that exist examining Hg transport and fate in aquifers (Lamborg et al., 2013).

Table 2: Theoretical (liquid-phase THg mass-balance) and measured solid-phase THg concentrations and recoverys of the measured-to-expected (theoretical) concentrations for each the columns in EXP1 and EXP2.

Experiment 1 (EXP1; 46.1 ± 1.1 mg L^{-1})					Experiment 2 (EXP2; 144 ± 6 mg L^{-1})				
Column	Stage	Theoretical Hg conc. (mg kg^{-1})	Measured Hg conc. (mg kg^{-1})	Recovery	Column	Stage	Theoretical Hg conc. (mg kg^{-1})	Measured Hg conc. (mg kg^{-1})	Recovery
C1.1	Desorption	820	722 ± 91	88.0%	C2.1	Desorption	1360	1060 ± 230	78.3%
C1.2	Desorption	890	877 ± 206	98.6%	C2.2	Desorption	1300	786 ± 390	60.2%
C1.3	Desorption	847	835 ± 120	98.6%	C2.3	Desorption	1490	1050 ± 57	70.1%
C1.4	Equilibrium	1870	1470 ± 221	78.5%	C2.4	50% breakthrough	1030	785 ± 220	76.1%
C1.5	Equilibrium	1910	1630 ± 286	85.1%	C2.5	50% breakthrough	1140	702 ± 330	61.4%
C1.6	Equilibrium	1870	1440 ± 92	77.1%	C2.6	Equilibrium	2770	2380 ± 452	86.1%
C1.7	50% breakthrough	1320	1470 ± 384	111.3%	C2.7	Equilibrium	2850	2320 ± 388	81.2%
C1.8	50% breakthrough	1300	960 ± 524	73.6%	C2.8	Equilibrium	2820	2260 ± 272	79.8%

Measured THg concentrations were typically lower than the theoretical calculated values (Table 2) and contaminant masses can be difficult to balance in contaminant batch and column experiments (Van Genuchten and Parker, 1984; Hebig et al., 2014). This is of particular concern for a contaminant such as Hg whose stability and contamination issues have been widely studied due to the capacity of different Hg species to sorb to and diffuse through plastic polymers (at differing rates) (Hall et al., 2002; Parker and Bloom, 2005; Hammerschmidt et al., 2011). Loss of a fraction of the THg in solution to/through tubing and the walls of the column is likely contributing to the lower recovery in some of these samples. Other factors that could be contributing to the differences between the theoretical and measured concentrations are heterogeneity of the solid-phase and solid-phase sample extraction (particularly during movement of the Hg mass transfer front), loss of Hg from solid-phase before sample extraction and analyses (particularly for volatile Hg(0); Parker and Bloom, 2005), and inherent analytical uncertainties. The heterogeneity of the materials is emphasized by the absence of trends in THg concentrations within the sections of the columns, even for the columns undergoing movement of the mass transfer zone (see Section S8). Unfortunately, Miretzky et al. (2005) did not provide total sampling volumes for their experiments and no assessment of measured THg recoveries was (or can be) made for direct comparison to our recovery data.

3.1.2 Desorption

The desorption phase of both EXP1 and EXP2 followed an exponential decay model; results confirm that sorption is (partially) reversible and initially rapid (Figure 2). After the stock solution was

switched to water for the desorption phase, the eluate solution reached <50% of the stock solution THg concentration with additions of ≈1 L (≈43 pore volumes) and ≈0.5 L (≈22 pore volumes) of solution in EXP1 and EXP2, respectively (Figure 2). At the termination of the experiments eluate THg concentrations dropped to <10% of the original stock solution (Figure 2). While it is evident that more Hg would have been released if desorption was permitted to proceed further (terminated due to time and to prevent excess contaminated waste solution), measured data indicated that 46 ± 6% (Theoretical: 55 ± 2%) in EXP1 and 58 ± 10% (Theoretical: 51 ± 4%) in EXP2 of THg could be extracted from the solid-phase materials before the experiments were terminated. Evidence from the contaminated aquifer where these solid-phase materials were extracted suggest that the retention of a fraction of this Hg within the solid-phase materials is long-term (Bollen et al., 2008; McLagan et al., 2022). McLagan et al. (2022) report that elevated solid- (up to 562 mg kg^{-1}) and liquid-phase (up to 164 ± 75.4 µg L^{-1}) THg concentrations are still found at the site to the present day, more than 55 years since the industrial use of Hg (kyanisation) at the site ceased.

~~The authors of that~~McLagan et al. (2022) ~~study~~ associate this residual retention of Hg to the diffusion of Hg into the mineral matrix or secondary transformation to a more stable (and less soluble) Hg(II) species (McLagan et al., 2022). Previous work agrees that sorption and subsequent release of Hg to/from solid-phase soils and solid-phase materials is likely controlled by multiple processes (Yin et al., 1997; Bradl, 2004; Reis et al., 2016). The more easily extractable Hg is likely to be associated with Fe and Mn (oxy)hydroxide, and clay minerals through outer-sphere complexes that form through cation exchange and electrostatic intermolecular forces (Bradl, 2004; Reis et al., 2016). Over time, some of the Hg associated through these weaker surface interactions will diffuse into the matrix and/or form inner-sphere complexes, processes that both slow the release of the sorbed Hg (Bradl, 2004; Reis et al., 2016). Similar results were observed by Miretzky et al. (2005) in the OM rich Amazonian soil columns with 27 - 38% of Hg sorbed to the solid-phase materials being rapidly redissolved in the initial desorption phase. However, the soils with higher OM content showed stronger hysteresis and considerably less Hg was released during the second phase of desorption (Miretzky et al., 2005) than in our low OM solid-phase materials suggesting stronger interactions of inner-sphere complexed Hg with OM; results supported by work done in other studies examining Hg sorption to solid-phase materials (Yin et al., 1996; Reis et al., 2016).

3.1.3 Insights from stable Hg isotopes

Variations in δ^{202}Hg values, describing MDF of Hg isotopes, were observed in both the liquid- and solid-phase across the experiments (Figure 3; Section S7; Section S8). During the initial phase of the experiments (before eluate breakthrough), transfer of Hg from the applied stock solution (δ^{202}Hg: -0.61 ± 0.01‰ relative to NIST-3133, 1SD; *n* = 3) to the solid-phase materials is complete. When there is complete transfer of a "pool" of Hg from reactants to products there is complete transfer of stable isotopes; and hence no fractionation can be observed.

Once Hg begins to breakthrough the columns, the eluate is initially enriched in heavy isotopes associated with the preferential transfer (sorption) of lighter isotopes to the solid-phase materials (Jiskra et al., 2012; Wiederhold, 2015) with heavier isotopes retained in solution ~~and~~ (passed into the eluate). In all three of the EXP2 columns examined for stable isotopes in the liquid-phase, the first two liquid-phase stable isotope samples (sampled just after ≈50% breakthrough column removals) had more positive δ^{202}Hg values than the remaining liquid-phase samples (Figure 3). However, it is also apparent that at ≈50% breakthrough, there was little MDF imparted on the solid-phase materials compared to the stock solution (Figure 3). This ostensibly contrasting finding

(observable positive MDF in the liquid-phase and little negative MDF in the solid-phase) can be explained by the proportion of Hg transferred to the solid-phase of the total mass added in solution. At the 50% breakthrough column removal, the proportion of Hg sorbed by the columns was 95.4 and 90.4%, respectively for C1.7 and C1.8 (EXP1) and 83.8 and 88.5%, respectively for C2.4 and C2.5 (EXP2; based on theoretical calculations). The majority of this sorption occurred during the complete (or near-complete) transfer of isotopes before (or just after) eluate breakthrough. Hence, the MDF that began to occur after breakthrough (observable in the early liquid-phase eluate samples) had little influence on the Hg stable isotope ratios of the solid-phase materials of columns removed at the ≈50% breakthrough point.

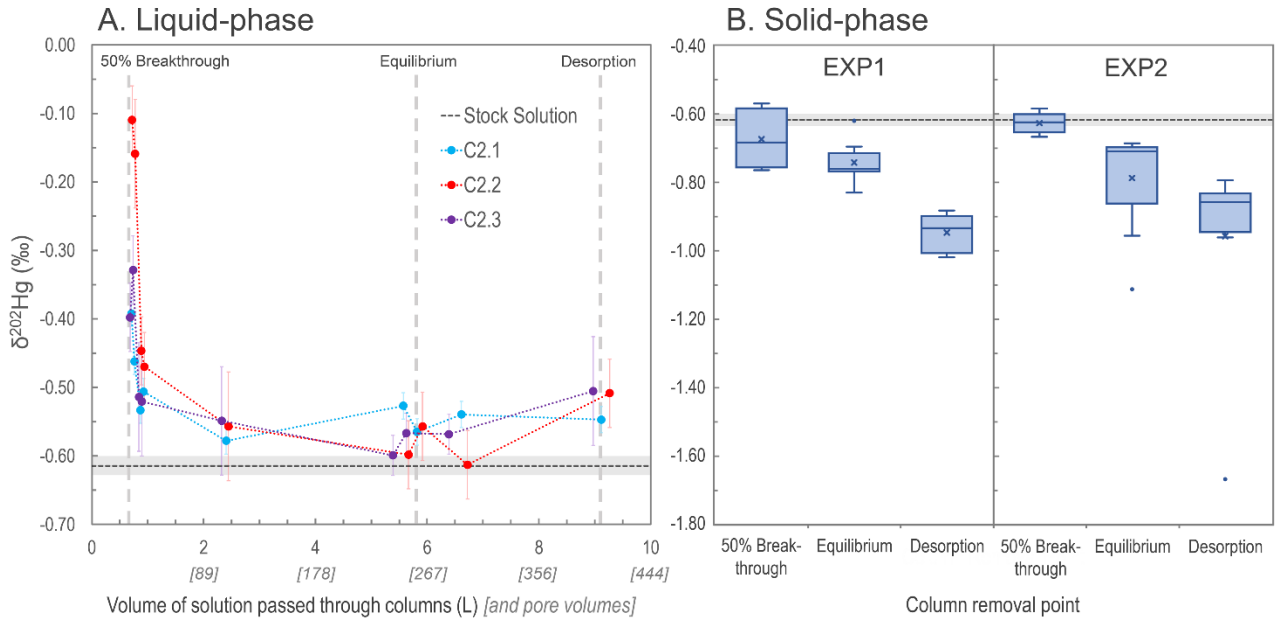

Figure 3: Development of liquid-phase δ^{202}Hg values for columns C2.1 – C2.3 measured at nine intervals during EXP2 (Panel A).~~and b~~Box plots of solid-phase δ^{202}Hg values measured in both EXP1 and EXP2 ("x" denotes mean values, dots denote outliers) (Panel B). In both panels, the grey dash line represents the mean δ^{202}Hg value (light grey rectangle: 1SD) measured for the stock solution. Note, the vertical grey dashed lines indicating solid-phase column removal points in the left panel are only approximations as the liquid-phase stable isotope measurements were only made on columns C2.1-2.3 that proceeded until the end of desorption.

This ~~process~~ finding of limited MDF on solid phase materials at ≈50% breakthrough is ~~further supported when examining~~consistent with the δ^{202}Hg values observed within~~of~~ the column layers ~~at ≈50% breakthrough~~. The bottom layers of C1.7 (δ^{202}Hg: -0.76 ± 0.07‰) and C1.8 (δ^{202}Hg: -0.75 ± 0.07‰) in EXP1 were more negative than the stock solution, while the top layers (δ^{202}Hg: -0.57 ± 0.15‰ and δ^{202}Hg: -0.59 ± 0.07‰ for C1.7 and C1.8, respectively) were equivalent to the stock solution (Section S8). These data suggest observable MDF was beginning to occur in the part of the column exposed to the Hg front (bottom) for the longest. The same was not the case in EXP2 (no observable trend in δ^{202}Hg between layers; Section S8). We attribute this to the more elevated THg concentrations and faster movement of the Hg front moving through the columns (see Table 3 below) in EXP2 overwhelming the layering MDF observed in EXP1.

As sorption progresses to equilibrium, we observe a negative shift in the eluate δ^{202}Hg value of all three columns falling in the range of ≈-0.6 to -0.5‰, which is slightly more positive than the stock solution (δ^{202}Hg: -0.61 ± 0.01 ‰ 1SD; ± 0.08 ‰ analytical 2SD; Figure 3). During this transition in the

Hg uptake process the net effect is that most, and then essentially all, Hg input from the stock solution is passing through the columns and into the eluate and any kinetic MDF occurring would be limited. Nonetheless, equilibrium-based isotope exchange would also drive lighter isotopes into the solid-phase materials (Wiederhold et al., 2010; Jiskra et al., 2012; Wiederhold, 2015), which is the likely explanation for the liquid-phase δ^{202}Hg values remaining slightly more positive than the stock solution. While the impact of this MDF on the continuously flowing eluate is small when the system is at equilibrium, the effect of this equilibrium-based MDF on the solid-phase is more manifest as its effect is cumulative. Over time, more and more lighter isotopes preferentially sorb to the solid-phase; and hence, the mean δ^{202}Hg values of the solid-phase materials in EXP1 (δ^{202}Hg: -0.74 ± 0.06‰ 1SD) and EXP2 (δ^{202}Hg: -0.79 ± 0.15‰ 1SD) at the end of the sorption experiments (at or near column equilibrium) are more negative than the stock solution (and solid-phase materials at ≈50% breakthrough). Thus, we suggest equilibrium-based MDF (with some potential for kinetic MDF contributions) to be the primary driver of the more negative δ^{202}Hg values observed in the solid-phase materials at the end of the equilibrium-phase of the experiments. These observations agree with the observed results of McLagan et al. (2022) sampled within the contaminated aquifer adjacent to which these uncontaminated materials were derived.

At the end of the desorption phase, the solid-phase materials have undergone further MDF to more negative δ^{202}Hg values (EXP1 δ^{202}Hg: -0.95 ± 0.05‰; EXP2 δ^{202}Hg: -0.96 ± 0.27‰ 1SD). Two of the three columns monitored for liquid-phase stable isotopes at the end of desorption also show a slight positive MDF shift and values for all three columns are slightly more positive (δ^{202}Hg: -0.55 to -0.51 ‰) than the stock solution (Figure 3). As discussed, desorption proceeds via a two-step mechanism: a rapid initial desorption as easily exchangeable, outer-sphere complexed Hg is released, followed by a slower phase of desorption as this easily exchangeable pool depletes. Brocza et al. (2019) and McLagan et al. (2022) suggest that this easily exchangeable pool is enriched in heavier isotopes compared to the fraction that diffuses into the mineral matrix or transforms to more stable, less soluble Hg(II) species as these secondary processes favour lighter isotopes. Thus, removal of the heavy isotope enriched, easily exchangeable pool of Hg is the likely driver of more negative δ^{202}Hg values in the solid-phase materials after desorption. While Demers et al. (2018) studied predominantly surface water samples linked to Hg soil-groundwater contamination at a site in Tennessee, USA (industrial use of Hg(0)), they did observe more positive δ^{202}Hg values with elevated dissolved THg concentrations values in samples from the hyporheic zone associated with exfiltrating groundwater from the contaminated areas. These data would agree with the more positive liquid-phase δ^{202}Hg values observed in our study and by McLagan et al. (2022).

Variation in both odd- and even-isotope MIF was within the range of analytical uncertainties (Section S7; Section S8). McLagan et al. (2022) did observe small variation in Δ^{199}Hg between solid- and liquid-phases, which the authors suggest may be linked to MIF driven by dark abiotic reduction of Hg(II) (Zheng and Hintelmann, 2010). However, it is unlikely that this process could manifest into an observable change in Δ^{199}Hg considering the short duration of these experiments even if the process could occur at all within these columns.

3.2 Is reduction of Hg(II) to Hg(0) occurring within the columns?

Reduction of Hg(II) to Hg(0) has been observed previously at this and other sites impacted by kyanisation activities (Bollen et al., 2008; Richard et al., 2016a; 2016b; McLagan et al., 2022). In these subsurface environments with low OM and very high THg concentrations, this secondary Hg(0)

production has been linked to abiotic, (hydr)oxide mineral surface catalysed reactions driven by other redox active metals (Bollen et al., 2008; Richard et al., 2016a; 2016b; Schwab et al., 2023). Since $HgCl_2$ solution was the only form of Hg applied in the column experiments, the presence of Hg(0) in either the liquid- or solid-phases must be explained via reduction of Hg(II).

To examine the presence of Hg(0), PTD analyses were run on the (undried) solid-phase materials from the columns after the sorption experiments. The PTD extinction curves showed little variation across all sections of all columns from either experiment (see Section S9). All curves mimic the low sample weight (≈0.1 g) mean extinction curves displayed in Figure 4 and are dominated by a single peak with a maximum release of ≈225 °C, which aligns with the maximum extinction of the $HgCl_2$ standard in silicon dioxide (SiO_2). This supports the hypothesis of direct (outer-sphere) complexation or electrostatic interaction of dissolved Hg(II) species to the mineral surfaces posited previously (Bradl, 2004; Reis et al., 2016) and by McLagan et al. (2022). Nonetheless, these low sample weight PTD curves were indicative of some qualitative evidence of very small peaks at <175 °C (Section S9); peaks in this range are associated with Hg(0) (Biester and Scholz, 1996; McLagan et al., 2022). The initial sample masses used in the PTD analyses were low (≈0.1 g) so as to not overwhelm the AAS detector, release large amounts of gas-phase Hg(0), and potentially cause memory effects in future analyses. Nevertheless, this would not occur if sample masses were increased (≈2.0 g) and the temperature ramp stopped at ≈175 °C. When the solid-phase materials were analysed in this manner, Hg(0) peaks were detected across all sections of all columns in both experiments (see Section S9; Figure 4).

Additionally, detectable concentrations of Hg(0) were observed across all of the ~~qualitative~~ semi-quantitative liquid-phase Hg speciation analyses and elevated above the Hg(0) concentrations measured in the stock solution (Section S4). The observed liquid-phase fraction of Hg(0) was highest at the ≈25% breakthrough sample collection point in EXP1 (0.7%) and EXP2 (0.1%) with the fraction being ≤0.1% in all other samples (Section S4). While these data suggest that reduction of Hg(II) to Hg(0) begins almost immediately after the introduction of the $HgCl_2$ solution, we link the declining proportion of Hg(0) to the low solubility of Hg(0) (≈50 µg L^{-1}) (Skyllberg, 2012; Brocza et al., 2019), which was already reached at the ≈25% breakthrough sample collection point in both experiments.

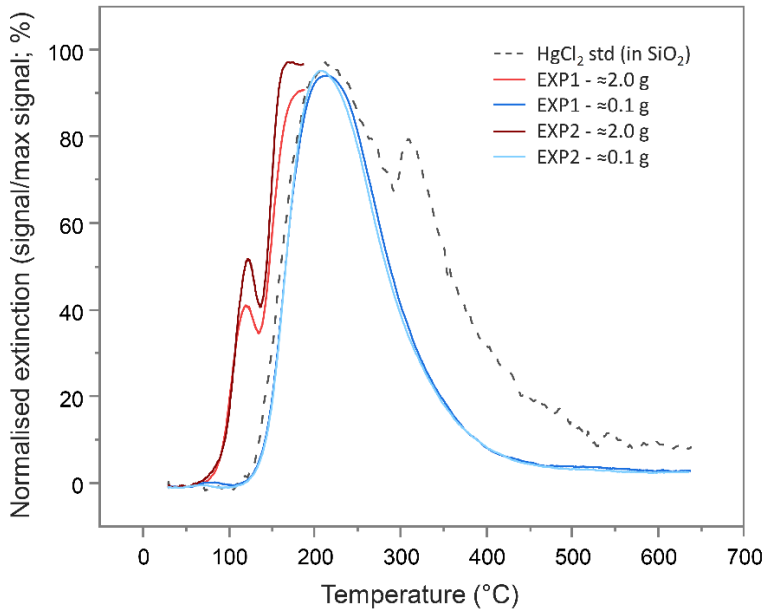

Figure 4: Mean pyrolytic thermal desorption (PTD) extinction curves from solid-phase materials from EXP1 and EXP2 assessed with two different sample masses. Analyses of the larger sample mass (≈2.0 g of material) were terminated when the temperature ramp reached ≈175 °C to prevent excessive gas-phase Hg release and potential memory effects on the instrument.

These measured Hg(0) fractions in solid- and liquid-phase analyses provide further direct evidence of Hg(0) production under saturated, oxic conditions in low OM solid-phase materials. Hg(0) production in these contaminated aquifers has been linked to the slower than expected horizontal progress of the plume of Hg in the aquifer at the site where this contamination occurred (Bollen et al., 2008; Richard et al., 2016a; 2016b; McLagan et al., 2022). While these data indicate that the fraction of Hg(0) produced is relatively small, the volume of soil and aquifer materials in which this process can occur is large. The contamination plume of the aquifer at the site where the solid phase materials were removed from is ≈1000 m long and covers ~~with~~ an area of ≈6x10^4 m^2 (Bollen et al., 2008; McLagan et al., 2022). If we ~~conservatively~~ assume conservative values for~~a~~ mean depth of contamination of 2 m (aquifer ≈3-4 m depth; Bollen et al., 2008; McLagan et al., 2022), mean THg concentration of 2 mg kg^{-1} (solid phase THg concentration of 2-162 mg kg^{-1} along the contaminated aquifer; Bollen et al., 2008), the fraction of Hg(0) produced per day is 0.01 – 0.001% of the THg (based off 0.1% Hg(0) peak integration of total peak area of mean PTD curve from EXP2; see Section S9) ~~(all conservative estimates) based off data from Bollen et al., 2008; McLagan et al., 2022)~~, and the same bulk density and flow rates as in our experiments, we can produce a *back-of-the-envelope* estimate of the mass of Hg(0) produced and potentially lost from the aquifer to overlying soils. Based off these numbers, we estimate that 0.3 – 0.4 g of Hg(II) is transformed to Hg(0) each day within the aquifer of the contaminated site in southern Germany; over the course of one-year, this equates to the transformation ≈5 – 15 kg of Hg(II) to Hg(0). Even a relatively conservative estimate of the conversion (and potential loss) of this mass of Hg(II) in contaminated aquifers such as this provides strong evidence that the process of Hg(II) reduction plays a key role in limiting the transport of the 10-20 tonnes of Hg that was added to this soil-groundwater system in the ≈120 years since industrial operations commenced.

3.3 Retardation (R_D) and sorption coefficient (K_D) calculations

As expected, R_D values were substantially greater than 1, confirming substantial interaction between the applied $HgCl_2$ solution and the solid-phase aquifer materials (Table 3). The difference in R_D and K_D values between EXP1 and EXP2 (Table 3) indicate stock solution concentration is a factor in the transport of mercury within these columns. The elevated stock solution concentrations may be undermining the assumption of equal accessibility to sorption sites (USEPA, 2004). However, the purpose of these experiments was to simulate the original contamination by the industrial (mis)use~~/misuse~~ of $HgCl_2$ solution, and while we can only estimate original concentration of solution being transported through the soil-groundwater system, we do expect they were very high due to the extent (both in terms of elevated concentrations and longitudinal and transverse dispersion ~~three-dimensional spread~~ of the contamination plume) of contamination that remains and the very high concentration of the solution used in rot-prevention treatment of timber (Bollen et al., 2008; Richard et al., 2016a; McLagan et al., 2022). Considering the high concentrations of Hg that have been observed within this and other Hg contaminated aquifers (Katsenovich et al., 2010; Lamborg et al., 2013; Demers et al., 2018), it is critical that we do not isolate our study of Hg transport dynamics to low concentration experiments that meet assumptions for theoretical sorption (batch and column) experiments.

Table 3: Calculated retardation (R_D) and sorption (K_D) coefficients for EXP1 and EXP2 (definitions are given in Section 2.2.5).

EXP1					EXP2				
Column	t_w (min)	t_{Hg} (min)	R_D	K_D (mL g^{-1})	Column	t_w (min)	t_{Hg} (min)	R_D	K_D (mL g^{-1})
C1.1	48.9	3628	74.7	23.8	C2.1	43.0	1615	37.6	11.8
C1.2	41.0	3629	88.5	29.5	C2.2	38.2	1567	41.2	12.9
C1.3	50.0	3779	75.6	25.1	C2.3	45.8	1837	39.9	12.6
C1.4	49.5	3678	74.3	-	C2.6	41.0	1438	35.1	-
C1.5	44.0	3488	79.3	-	C2.7	44.1	1623	36.9	-
C1.6	47.8	3599	75.3	-	C2.8	37.5	1317	35.1	-
		Mean	**77.9**	**26.1**			**Mean**	**38.4**	**12.4**
		SD	**5.5**	**3.0**			**SD**	**2.7**	**0.6**

R_D values can be calculated from Miretzky et al. (2005) based on the inverse of their V/V_{water} value and the mean of these derived R_D values is 48 ± 13 for the high OM Amazonian soils. This again affirms the high sorptive capacity of our low OM solid-phase aquifer materials at these comparative concentration $HgCl_2$ applications. Lamborg et al. (2013) calculated K_D values for a Hg contaminated (from wastewater treatment) aquifer between 100 and 6300 mL g^{-1} (log K_D: 2-3.8); yet calculations had to assume liquid-phase concentrations from other studies. Log K_D values calculated from soil and sediment batch experiments typically range from ≈2 in lower OM materials (Akcay et al., 1996) up to ≈6 in higher OM materials (Lyon et al., 1997). The logical next step is to utilise the measured R_D and K_D data from our study to perform soil-groundwater modelling to better understand Hg transport in this and other soil-groundwater systems as there are no previous estimates of R_D and K_D values based on measured data for low OM solid-phase aquifer materials. The range of coefficient values from ours and other studies described above relating to differing solid-phase properties, input solution speciation, and assumptions used highlights the caution that should be made applying these values to other systems as R_D and K_D values tend to be highly site specific (USEPA, 2004).

Acknowledgements

We would like to thank Adelina Calean and Petra Schmidt for their support and contributions in terms of experimental setup and sample analyses (including A.C. travelling to Vienna for to assist with isotope analyses). We also thank undergraduate students Jan Pietrucha, Jette Greiser, and Katja Braun for helping with liquid-phase sample collection and analyses. We thank Stephan M. Kraemer for supporting the Hg isotope analyses at the University of Vienna. We would also like to acknowledge Thomas Schöndorf from HPC Environmental Consulting for providing the solid-phase materials used in this study. Also thanks to Hans Esser for helping design the eight-column holding rack used in the experiments. This research was funded by the German Science Foundation (DFG) grant BI 734/17-1 to H.B. and the Austrian Science Fund (FWF) grant I-3489-N28 to J.W. D.S.M. would like to thank for support provided through a National Sciences and Engineering Research Council of Canada (NSERC) postdoctoral fellowship.

Author contributions

D.S.M., C.E., and H.B. designed the study and experiments with some feedback from other co-authors, particularly J.-H.R during preliminary experiments. C.E. led all concentration and speciation analyses with assistance from D.S.M. Isotope analyses were led by L.S. with assistance from J.W. (and A.C. see above). This work was the basis for C.E.'s master's thesis, which was written in German. The manuscript first draft was written by D.S.M. and all other authors provided feedback in building the manuscript towards submission. Figures, tables, and SI were produced by D.S.M, C.E., and L.S.

References

Andersson, A.: Mercury in soil, In: The biochemistry of mercury in the environment, edited by: Nriagu, J. O., Elsevier, Amsterdam, Holland, 79-112, ISBN: 0444801103, 1979.

Akcay, H., Kilinç, S. İ. B. E. L., and Karapire, C.: A comparative study on the sorption and desorption of Hg, Th and U on clay, J. Radioanal. Nucl. Chem., 214, 51-66, https://doi.org/10.1007/bf02165058, 1996.

Avotins, P. V.: Adsorption and coprecipitation studies of mercury on hydrous iron oxide, Stanford University, Stanford, USA, ISBN: 9798660526602, 1975.

Bergquist, B. A., and Blum, J. D.: Mass-dependent and-independent fractionation of Hg isotopes by photoreduction in aquatic systems, Science, 318, 417-420, https://doi.org/10.1126/science.1148050, 2007.

Bergquist, B. A., and Blum, J. D.: The odds and evens of mercury isotopes: applications of mass-dependent and mass-independent isotope fractionation, Elements, 5, 353-357, https://doi.org/10.2113/gselements.5.6.353, 2009.

Bloom, N. S., Preus, E., Katon, J., and Hiltner, M.: Selective extractions to assess the biogeochemically relevant fractionation of inorganic mercury in sediments and soils, Anal. Chim. Acta, 479, 233-248, https://doi.org/10.1016/S0003-2670(02)01550-7, 2003.

Bollen, A., Wenke, A., and Biester, H.: Mercury speciation analyses in $HgCl_2$-contaminated soils and groundwater—implications for risk assessment and remediation strategies, Water Res., 42, 91-100, https://doi.org/10.1016/j.watres.2007.07.011, 2008.

Brocza, F. M., Biester, H., Richard, J. H., Kraemer, S. M., and Wiederhold, J. G.: Mercury isotope fractionation in the subsurface of a Hg(II) chloride-contaminated industrial legacy site, Environ. Sci. Technol., 53, 7296-7305, https://doi.org/10.1021/acs.est.9b00619, 2019.

Bradl, H. B.: Adsorption of heavy metal ions on soils and soils constituents, J. Colloid Interf. Sci., 277, 1-18, https://doi.org/10.1016/j.jcis.2004.04.005, 2004.

Clarkson, T. W.: The toxicology of mercury, Crit. Rev. Clinic. Lab. Sci., 34, 369-403, https://doi.org/10.3109/10408369708998098, 1997.

Demers, J. D., Blum, J. D., Brooks, S. C., Donovan, P. M., Riscassi, A. L., Miller, C. L., Zheng, W. and Gu, B.: Hg isotopes reveal in-stream processing and legacy inputs in East Fork Poplar Creek, Oak Ridge, Tennessee, USA, Environ. Sci. Process. Impacts, 20, 686-707, https://doi.org/10.1039/C7EM00538E, 2018.

DIN ISO: Method 11277: Soil quality–Determination of particle size distribution in mineral soil material–Method by sieving and sedimentation, German Institute for Standardisation (Deutsches Institut für Normung; DIN) International Organization for Standardization (ISO), Berlin, Germany, 2002.

DIN: Method 1483: Water quality - Determination of mercury - Method using atomic absorption spectrometry, German Institute for Standardisation (Deutsches Institut für Normung; DIN), Berlin, Germany, 2007.

DIN: 19528-01: Leaching of solid materials - Percolation method for the joint examination of the leaching behaviour of organic and inorganic substances for materials with a particle size up to 32 mm - Basic characterization using a comprehensive column test and compliance test using a quick column test, German Institute for Standardisation (Deutsches Institut für Normung; DIN), Berlin, Germany, 2009.

Gabriel, M. C., and Williamson, D. G.: Principal biogeochemical factors affecting the speciation and transport of mercury through the terrestrial environment, Environ. Geochem. Health, 26, 421-434, https://doi.org/10.1007/s10653-004-1308-0, 2004.

Gettens, R. J., Feller, R. L., and Chase, W. T.: Vermilion and cinnabar. Stud. Conserv., 17, 45-69, https://doi.org/10.1179/sic.1972.006, 1972.

Goix, S., Maurice, L., Laffont, L., Rinaldo, R., Lagane, C., Chmeleff, J., Menges, J., Heimbürger, L.E., Maury-Brachet, R. and Sonke, J. E.: Quantifying the impacts of artisanal gold mining on a tropical river system using mercury isotopes, Chemosphere, 219, 684-694, https://doi.org/10.1016/j.chemosphere.2018.12.036, 2019.

Grigg, A. R., Kretzschmar, R., Gilli, R. S., and Wiederhold, J. G.: Mercury isotope signatures of digests and sequential extracts from industrially contaminated soils and sediments, Sci. Tot. Environ., 636, 1344-1354, https://doi.org/10.1016/j.scitotenv.2018.04.261, 2018.

Gu, B., Bian, Y., Miller, C. L., Dong, W., Jiang, X., and Liang, L.: Mercury reduction and complexation by natural organic matter in anoxic environments, Proceed. Nat. Acad. Sci., 108, 1479-1483, https://doi.org/10.1073/pnas.1008747108, 2011.

Gunneriusson, L. and Sjöberg, S.: Surface complexation in the H+-goethite (α-FeOOH)-Hg (II)-chloride system, J. Colloid Interf. Sci. 156, 121-128, https://doi.org/10.1006/jcis.1993.1090, 1993.

721 Haitzer, M., Aiken, G. R., and Ryan, J. N.: Binding of mercury (II) to dissolved organic matter: the role
722 of the mercury-to-DOM concentration ratio, Environ. Sci. Technol., 36, 3564-3570,
723 https://doi.org/10.1021/es025699i, 2002.

724 Hall, G. E., Pelchat, J. C., Pelchat, P., and Vaive, J. E.: Sample collection, filtration and preservation
725 protocols for the determination of 'total dissolved' mercury in waters, Analyst, 127, 674-680,
726 https://doi.org/10.1039/B110491H, 2002.

727 Hammerschmidt, C. R., Bowman, K. L., Tabatchnick, M. D., and Lamborg, C. H.: Storage bottle
728 material and cleaning for determination of total mercury in seawater, Limnol. Oceanogr.
729 Methods, 9, 426-431, https://doi.org/10.4319/lom.2011.9.426, 2011.

730 Hebig, K. H., Nödler, K., Licha, T., and Scheytt, T. J.: Impact of materials used in lab and field
731 experiments on the recovery of organic micropollutants, Sci. Tot. Environ., 473, 125-131,
732 https://doi.org/10.1016/j.scitotenv.2013.12.004, 2014.

733 Ho, T. L.: Hard soft acids bases (HSAB) principle and organic chemistry, Chem. Rev., 75, 1-20,
734 https://doi.org/10.1021/cr60293a001, 1975.

735 Jiskra, M., Wiederhold, J. G., Bourdon, B., and Kretzschmar, R.: Solution speciation controls mercury
736 isotope fractionation of Hg(II) sorption to goethite. Environ. Sci. Technol., 46, 6654-6662,
737 https://doi.org/10.1021/es3008112, 2012.

738 Jiskra, M., Wiederhold, J. G., Skyllberg, U., Kronberg, R. M., and Kretzschmar, R.: Source tracing of
739 natural organic matter bound mercury in boreal forest runoff with mercury stable isotopes, Environ.
740 Sci. Process. Impacts, 19, 1235-1248, https://doi.org/10.1039/C7EM00245A, 2017.

741 Katsenovich, Y., Tachiev, G., Fuentes, H. R., Roelant, D., and Henao, A.: A study of the mercury (II)
742 sorption and transport with Oak Ridge Reservation soil, Waste Management Conference 2010,
743 Phoenix, USA, https://archivedproceedings.econference.io/wmsym/2010/pdfs/10222.pdf, 2010.

744 Kim, C. S., Rytuba, J. J., and Brown Jr, G. E.: EXAFS study of mercury (II) sorption to Fe-and Al-(hydr)
745 oxides: II. Effects of chloride and sulfate, J. Colloid Interf. Sci., 270, 9-20,
746 https://doi.org/10.1016/j.jcis.2003.07.029, 2004.

747 Kocman, D., Horvat, M., Pirrone, N., and Cinnirella, S.: Contribution of contaminated sites to the
748 global mercury budget, Environ. Res., 125, 160-170, https://doi.org/10.1016/j.envres.2012.12.011,
749 2013.

750 Lamborg, C. H., Kent, D. B., Swarr, G. J., Munson, K. M., Kading, T., O'Connor, A. E., Fairchild, G. M.,
751 LeBlanc, D. R., and Wiatrowski, H. A.: Mercury speciation and mobilization in a wastewater-
752 contaminated groundwater plume, Environ. Sci. Technol., 47, 13239-13249,
753 https://doi.org/10.1021/es402441d, 2013.

754 Leterme, B., Blanc, P., and Jacques, D.: A reactive transport model for mercury fate in soil—
755 application to different anthropogenic pollution sources, Environ. Sci. Poll. Res., 21, 12279-12293,
756 https://doi.org/10.1007/s11356-014-3135-x, 2014.

757 Lewis, J., and Sjöstrom, J.: Optimizing the experimental design of soil columns in saturated and
758 unsaturated transport experiments, J. Contam. Hydrol., 115, 1-13,
759 https://doi.org/10.1016/j.jconhyd.2010.04.001, 2010.

760 Lockwood, R. A., and Chen, K. Y.: Adsorption of mercury (II) by hydrous manganese oxides, Environ.
761 Sci. Technol., 7, 1028-1034, https://doi.org/10.1021/es60083a006, 1973.

762 Llanos, W., Kocman, D., Higueras, P., and Horvat, M.: Mercury emission and dispersion models from
763 soils contaminated by cinnabar mining and metallurgy, J. Environ. Monit., 13, 3460-3468,
764 https://doi.org/10.1039/C1EM10694E, 2011.

765 Lu, Y. F., Wu, Q., Yan, J. W., Shi, J. Z., Liu, J., and Shi, J. S.: Realgar, cinnabar and An-Gong-Niu-Huang
766 Wan are much less chronically nephrotoxic than common arsenicals and mercurial, Exp. Biol.
767 Med., 236, 233-239, https://doi.org/10.1258/ebm.2010.010247, 2011.

768 Lyon, B. F., Ambrose, R., Rice, G., and Maxwell, C. J.: Calculation of soil-water and benthic sediment
769 partition coefficients for mercury, Chemosphere, 35, 791-808, https://doi.org/10.1016/S0045-
770 6535(97)00200-2, 1997.

771 Manceau, A., and Nagy, K. L.: Thiols in natural organic matter: Molecular forms, acidity, and
772 reactivity with mercury (II) from First-Principles calculations and high energy-resolution X-ray
773 absorption near-edge structure spectroscopy, ACS Earth Space Chem., 3, 2795-2807,
774 https://doi.org/10.1021/acsearthspacechem.9b00278, 2019.

775 McLagan, D. S., Schwab, L., Wiederhold, J. G., Chen, L., Pietrucha, J., Kraemer, S. M., and Biester, H.:
776 Demystifying mercury geochemistry in contaminated soil–groundwater systems with
777 complementary mercury stable isotope, concentration, and speciation analyses, Environ. Sci.
778 Process. Impacts, 24, 1406-1429, https://doi.org/10.1039/D1EM00368B, 2022.

779 Miretzky, P., Bisinoti, M. C., & Jardim, W. F.: Sorption of mercury (II) in Amazon soils from column
780 studies, Chemosphere, 60, 1583-1589, https://doi.org/10.1016/j.chemosphere.2005.02.050, 2005.

781 Norrby, L. J.: Why is mercury liquid? Or, why do relativistic effects not get into chemistry
782 textbooks? J. Chem. Ed., 68, 110, https://doi.org/10.1021/ed068p110, 1991.

783 Obrist, D., Agnan, Y., Jiskra, M., Olson, C. L., Colegrove, D. P., Hueber, J., Moore, C.W., Sonke, J.E.
784 and Helmig, D.: Tundra uptake of atmospheric elemental mercury drives Arctic mercury
785 pollution, Nature, 547, 201-204, https://doi.org/10.1038/nature22997, 2017.

786 Parker, J. L., and Bloom, N. S.: Preservation and storage techniques for low-level aqueous mercury
787 speciation, Sci. Tot. Environ., 337, 253-263, https://doi.org/10.1016/j.scitotenv.2004.07.006, 2005.

788 Patterson, B. M., Pribac, F., Barber, C., Davis, G. B., and Gibbs, R.: Biodegradation and retardation of
789 PCE and BTEX compounds in aquifer material from Western Australia using large-scale columns, J.
790 Contam. Hydrol., 14, 261-278, https://doi.org/10.1016/0169-7722(93)90028-Q, 1993.

791 Pirrone, N., Cinnirella, S., Feng, X., Finkelman, R.B., Friedli, H.R., Leaner, J., Mason, R., Mukherjee,
792 A.B., Stracher, G.B., Streets, D.G. and Telmer, K.: Global mercury emissions to the atmosphere from
793 anthropogenic and natural sources, Atmos. Chem. and Phys., 10, 5951-5964,
794 https://doi.org/10.5194/acp-10-5951-2010, 2010.

795 Reis, A. T., Davidson, C. M., Vale, C., and Pereira, E.: Overview and challenges of mercury
796 fractionation and speciation in soils, Trends Anal. Chem., 82, 109-117,
797 https://doi.org/10.1016/j.trac.2016.05.008, 2016.

Richard, J. H., Bischoff, C., and Biester, H.: Comparing modeled and measured mercury speciation in contaminated groundwater: Importance of dissolved organic matter composition, Environ. Sci. Technol., 50, 7508-7516, https://doi.org/10.1016/j.trac.2016.05.008, 2016a.

Richard, J. H., Bischoff, C., Ahrens, C. G., and Biester, H.: Mercury (II) reduction and co-precipitation of metallic mercury on hydrous ferric oxide in contaminated groundwater, Sci. Tot. Environ., 539, 36-44, https://doi.org/10.1016/j.scitotenv.2015.08.116, 2016b.

Sentenac, P., Lynch, R. J., and Bolton, M. D.: Measurement of a side-wall boundary effect in soil columns using fibre-optics sensing, Int. J. Phys. Model. Geotech., 1, 35-41, https://doi.org/10.1680/ijpmg.2001.010404, 2001.

Sanemasa, I.: The solubility of elemental mercury vapor in water, Bull. Chem. Soc. Jpn., 48, 1795-1798, https://doi.org/10.1246/bcsj.48.1795, 1975

Schroeder, W. H., and Munthe, J.: Atmospheric mercury—an overview, Atmos. Environ., 32, 809-822, https://doi.org/10.1016/S1352-2310(97)00293-8, 1998.

Schlüter, K., Seip, H. M., and Alstad, J.: Mercury translocation in and evaporation from soil. II. Evaporation of mercury from podzolized soil profiles treated with $HgCl_2$ and CH_3HgCl, Soil Sediment Contam., 4, 269-298, https://doi.org/10.1080/15320389509383498, 1995.

Schlüter, K.: Sorption of inorganic mercury and monomethyl mercury in an iron–humus podzol soil of southern Norway studied by batch experiments, Environ. Geol., 30, 266-279, https://doi.org/10.1007/s002540050156, 1997.

Schnaar, G., and Brusseau, M. L.: Measuring equilibrium sorption coefficients with the miscible-displacement method, J Environ. Sci. Health A, 48, 355-359, https://doi.org/10.1080/10934529.2013.727733, 2013.

Schöndorf, T., Egli, M., Biester, H., Mailahn, W., and Rotard, W.: Distribution, Bioavailability and Speciation of Mercury in Contaminated Soil and Groundwater of a Former Wood Impregnation Plant, in: Mercury Contaminated Sites, edited by: Ebinghaus, R., Turner, R.R., de Lacerda, L.D., Vasiliev, O., Salomons, W., Springer, Berlin, Heidelberg, 181-206, https://doi.org/10.1007/978-3-662-03754-6_9, 1999.

Schuster, E.: The behavior of mercury in the soil with special emphasis on complexation and adsorption processes-a review of the literature, Water Air Soil Poll., 56, 667-680, https://doi.org/10.1007/BF00342308, 1991.

Schuster, P. F., Shanley, J. B., Marvin-Dipasquale, M., Reddy, M. M., Aiken, G. R., Roth, D. A., Taylor, H. E., Krabbenhoft, D. P. and DeWild, J. F.: Mercury and organic carbon dynamics during runoff episodes from a northeastern USA watershed, Water Air Soil Poll., 187, 89-108, https://doi.org/10.1007/s11270-007-9500-3, 2008.

Schwab, L., Gallati, N., Reiter, S.M., Kimber, R.L., Kumar, N., McLagan, D.S., Biester, H., Kraemer, S.M. and Wiederhold, J.G.: Mercury Isotope Fractionation during Dark Abiotic Reduction of Hg (II) by Dissolved, Surface-Bound, and Structural Fe (II), Environ. Sci. Technol., 57, 15243-15254, https://doi.org/10.1021/acs.est.3c03703, 2023.

Skyllberg, U.: Chemical speciation of mercury in soil and sediment, in: Environmental chemistry and toxicology of mercury, edited by: Liu, G., Cai, Y., Driscoll, N., Wiley & Sons Inc., Hoboken, USA, 219-258, https://doi.org/10.1002/9781118146644.ch7, 2012.

839 Streets, D. G., Horowitz, H. M., Lu, Z., Levin, L., Thackray, C. P., and Sunderland, E. M.: Global and
840 regional trends in mercury emissions and concentrations, 2010–2015, Atmos. Environ., 201, 417-
841 427, https://doi.org/10.1016/j.atmosenv.2018.12.031, 2019.

842 Ullrich, S. M., Tanton, T. W., and Abdrashitova, S. A.: Mercury in the aquatic environment: a review
843 of factors affecting methylation, Crit. Rev. Environ. Sci. Technol., 31, 241-293,
844 https://doi.org/10.1080/20016491089226, 2001.

845 USEPA.: Method 1631, Revision E: Mercury in water by oxidation, purge and trap, and cold vapor
846 atomic fluorescence spectrometry, United States Environmental Protection Agency (USEPA),
847 Washington, DC, 2002.

848 USEPA.: Understanding variation in partition coefficient, Kd, values. Volume III: Review of
849 Geochemistry and Available Kd Values for Americium, Arsenic, Curium, Iodine, Neptunium, Radium,
850 and Technetium. United States Environmental Protection Agency (USEPA), Washington, DC, USA,
851 2004.

852 Van Genuchten, M. T., and Parker, J. C.: Boundary conditions for displacement experiments through
853 short laboratory soil columns, Soil Sci. Soc. Am. J., 48, 703-708,
854 https://doi.org/10.2136/sssaj1984.03615995004800040002x, 1984.

855 Van Glubt, S., Brusseau, M. L., Yan, N., Huang, D., Khan, N., and Carroll, K. C.: Column versus batch
856 methods for measuring PFOS and PFOA sorption to geomedia. Environ. Poll., 268, 115917,
857 https://doi.org/10.1016/j.envpol.2020.115917, 2021

858 Wiederhold, J. G., Cramer, C. J., Daniel, K., Infante, I., Bourdon, B., and Kretzschmar, R.: Equilibrium
859 mercury isotope fractionation between dissolved Hg (II) species and thiol-bound Hg, Environ. Sci.
860 Technol., 44, 4191-4197, https://doi.org/10.1021/es100205t, 2010.

861 Wiederhold, J. G.: Metal stable isotope signatures as tracers in environmental geochemistry,
862 Environ. Sci. Technol., 49, 2606-2624, https://doi.org/10.1021/es504683e, 2015.

863 Yin, Y., Allen, H. E., Li, Y., Huang, C. P., and Sanders, P. F.: Adsorption of mercury (II) by soil: effects
864 of pH, chloride, and organic matter, J. Environ. Qual., 25, 837-844,
865 https://doi.org/10.2134/jeq1996.00472425002500040027x, 1996.

866 Yin, Y., Allen, H. E., Huang, C., Sparks, D. L., and Sanders, P. F.: Kinetics of mercury (II) adsorption and
867 desorption on soil, Environ. Sci. Technol., 31, 496-503, https://doi.org/10.1021/es9603214, 1997.

868 Zheng, W., and Hintelmann, H.: Nuclear field shift effect in isotope fractionation of mercury during
869 abiotic reduction in the absence of light, J. Phys. Chem. A, 114, 4238-4245,
870 https://doi.org/10.1021/jp910353y, 2010.